Materials Science and Engineering A 378 (2004) 2–10

MATERIALS SCIENCE & ENGINEERING A

www.elsevier.com/locate/msea

High-temperature shape memory alloys Some recent developments

G.S. Firstov [a,b,*], J. Van Humbeeck [a], Y.N. Koval [b]

[a] *Department of MTM, Katholieke Universiteit Leuven, Kasteelpark Arenberg 44, B-3001 Leuven, Belgium*
[b] *Institute of Metal Physics of the National Academy of Sciences of Ukraine, 36 Vernadsky Street, 03142 Kiev-142, Ukraine*

Received 20 June 2003; received in revised form 11 October 2003

Abstract

Several alloy systems can be selected for high-temperature shape memory alloys (HTSMA) with stable transformation temperatures above 390 K. However, due to the lack of minimum quality standards for stability, ductility, functional behavior and reliability, no successful application have been realized so far.

This paper will cover some recent developments in design of the novel Zr–Cu-based HTSMA system through the comparison with Ti–Ni–Zr and Ti–Ni–Hf alloys. Important peculiarities in shape memory behaviour of HTSMA systems mentioned above will be emphasized. Chemical homogeneity for HTSMA systems under study as well as their martensitic transformation temperatures stability and oxidation resistance will be compared also. Finally, a comparison of the weak and strong parts of Zr–Cu-based, Ti–Ni–Zr and Ti–Ni–Hf HTSMA systems will be pointed out.

Keywords: Martensitic phase transformation; Shape memory alloys; High-temperature shape recovery

1. Introduction

Traditionally, the temperature interval of thermoelastic martensitic transformation in metals and alloys was observed at cryogenic and environmental temperatures (not more than 370 K). Therefore, the shape memory effect stimulated by the diffusionless character of the martensitic transformation has the appropriate characteristics in this temperature interval for the industrial shape memory alloys. The diffusion processes are suppressed at these temperatures, which ensures high reversibility during martensitic transformation.

Currently, robotic, automotive, aerospace industries and others need shape memory alloys that operate at temperatures higher than 390 K. In this case, martensitic (diffusionless) transformation (MT) takes place in a temperature range where diffusion controlled processes, such as decomposition, recrystallization, recovery, etc., cannot be neglected. In addition, it is necessary to alloy binary systems in order to adjust high temperatures of the martensitic transformation properly and to improve the ductility of the alloys. Such multi-component alloy systems are unstable to decomposition processes. Besides, the initial structure and microstructure of the alloys created by heat and thermal–mechanical treatments should affect the high-temperature shape memory behaviour.

The extensive research on Co-, Fe–Mn–Si-, Cu–Al–Ni-, Ni–Mn-, Ni–Al-, Ti–Pt (Pd, Au, Rh)- and Ni–Ti-based HTSMA reviewed in [1–4] was added significantly during the last decade. The HTSMA list mentioned above was replenished with Zr-based quasibinary [5–7], Ta–Ru and Nb–Ru binary [8–10] and Ni–Mn–Ga ternary [11] intermetallics. Expensive Ti–Pd–Ni HTSMA were still under investigation due to their good workability and high MT temperatures (up to 800 K) [3,12–17]. Still, the most attention was focussing on Ni–Ti–Zr and Ni–Ti–Hf HTSMA mainly due to the relative low prices for raw materials [18–30]. In this regard, Cu–Al–Ni alloys are still looking attractive (see [31], for example) if one does not need the shape recovery higher than 470 K. On the other hand, the Zr-based quasibinary intermetallics also can be considered competitive, as they appeared to show quite high temperatures of MT (up to 1100 K) associated with a decent high-temperature shape memory effect [5–7].

* Corresponding author. Tel.: +32-16-32-14-48; fax: +32-16-32-19-92.
E-mail address: feorgiy.firstov@mtm.kuleuven.ac.be (G.S. Firstov).

0921-5093/$ – see front matter © 2004 Elsevier B.V. All rights reserved.
doi:10.1016/j.msea.2003.10.324

The goal of the present paper is to perform an assessment of high-temperature shape memory behaviour and related properties for Ni–Ti–Zr, Ni–Ti–Hf and Zr–Cu-based quasibinary intermetallics, as they appear to be most hopeful candidates amongst the less expensive HTSMA.

2. Experimental

Zr–Cu–Ni–Co–Ti, Ti–Ni–Zr and Ti–Ni–Hf alloys were arc-melted from iodide Ti, Zr an Hf and electrolytic Co, Ni and Cu in a pre-gettered argon atmosphere and poured into a water-cooled copper mould. MT temperatures were detected with the help of TA 2920 differential scanning calorimeter using 5 K/min heating–cooling rate. Shape recovery was examined in TMA 934 dilatometer using 5 K/min heating–cooling rate after compression at a rate $2.8 \times 10^{-3}\ s^{-1}$ in an INSTRON 1196 equipped with furnace. Transmission electron microscopy was performed with help of a JEOL 100 CX device. The temperatures of melting and other phase transformations above 600 K were measured by a Netzsch 404 differential scanning calorimeter using 5 K/min heating rate. Scanning electron microscopy investigation of chemical inhomogeneity was carried out with a Philips XL30 FEG scanning electron microscope equipped with EDAX system. An IET device (RFDA, IMCE) described in [32,33] was used to investigate internal friction of plate-shaped specimens (nominal size 40 mm × 4 mm × 1 mm and weight 1 g suspended in the nodes of their first bending vibration mode. The Young's moduli are calculated from the bending resonance frequency f_r according to ASTM C 1259-94. Flat specimens for thermo-gravimetric measurements, 1.5 mm × 1.5 mm × 5 mm in dimension, were cut from the ingot, mechanically polished with emery paper to a mirror finish and ultrasonically cleaned in demineralized water and ethanol. Thermo-gravimetric measurements versus temperature were performed with the help of DuPont 951 TGA with a heating rate of 1 K/min under 50 ml/min air flow.

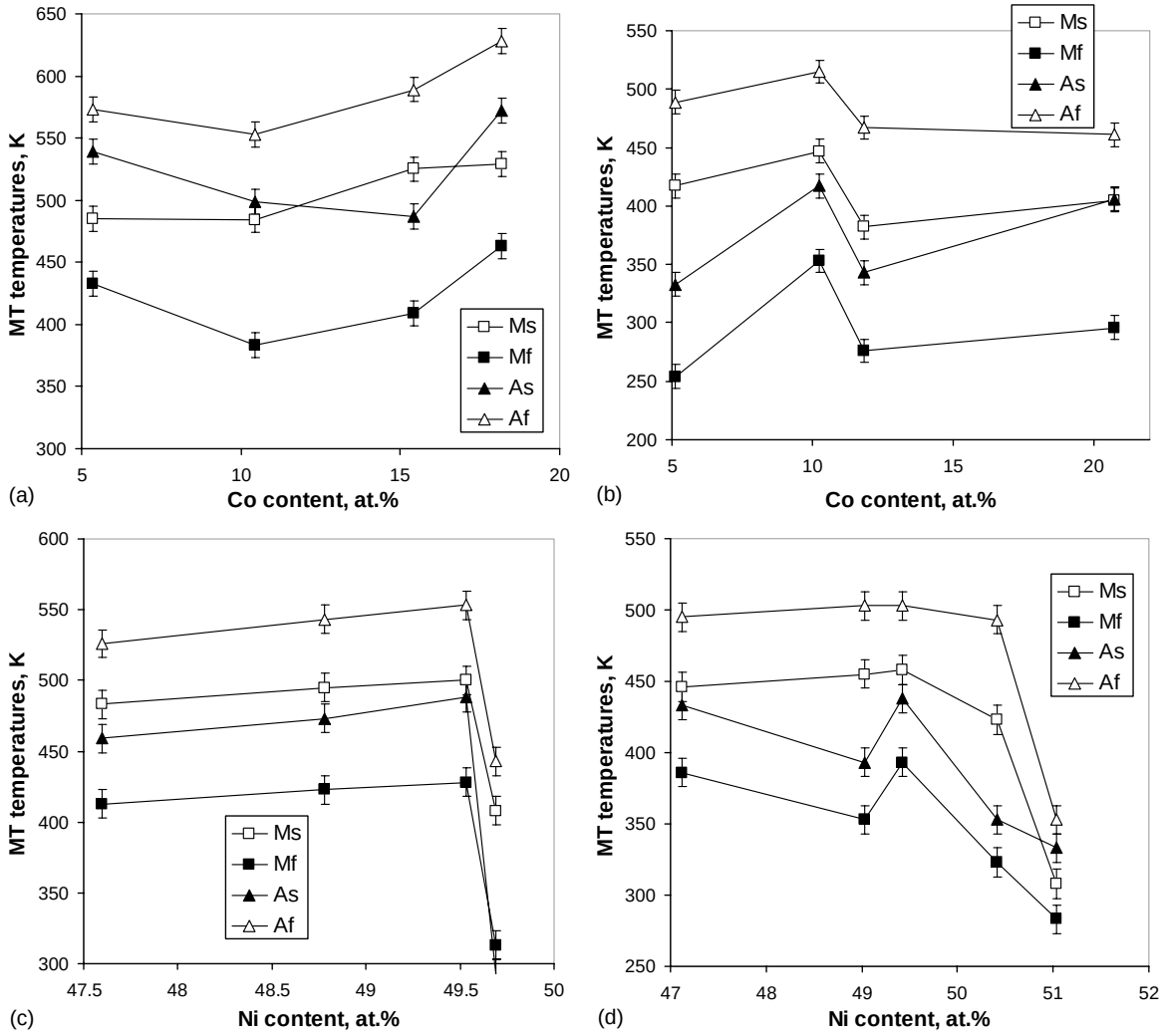

Fig. 1. MT temperatures measured by DSC vs. (a) Co content in $Zr_{50}Cu_{43-x}Ni_7Co_x$, (b) Co content in $Zr_{43}Cu_{39-x}Ni_{11}Co_xTi_7$, (c) Ni content in $Ti_{82-x}Ni_xZr_{18}$ and (d) Ni content in $Ti_{85.3-x}Ni_xHf_{14.7}$.

3. Results and discussion

In order to compare the shape memory potential of the alloys in question, their composition was adjusted in a way that all of them had M_s around 470 K. The actual temperatures of MT measured by DSC are shown in Fig. 1. It can be seen that Ti–Ni-based alloys with a constant amount of Zr (∼18 at.%) and Hf (∼14 at.%) are showing stable MT temperatures at high Ti content while the Ni amount is increasing up to ∼50 at.% of Ni with subsequent sharp decrease in MT temperatures (Fig. 1c and d), which is in good correspondence with data that can be found in [2], for example. As for Zr–Cu-based alloys, ternary Ni additions simply increased MT temperatures [34], while quaternary Co additions promoted the preferential formation of B19′ martensite [6] not changing MT temperatures significantly (Fig. 1a). Simultaneous substitution of Zr by Ti leads to a decrease in MT temperatures [34] and preferential formation of the martensite belonging to *Cm* space group, which is normally forming in binary Zr–Cu as the source of relaxation of the elastic energy alternative to lattice invariant shear [35]. That is the reason why in the case of Zr–Cu–Ni–Co–Ti alloys a slightly higher amount of Ni was necessary to keep M_s close to 470 K (Fig. 1b), while trying to use another than B19′ martensite for subsequent high-temperature shape recovery.

Deformation prior to shape recovery was applied at room temperature and after in situ heating above A_f temperature and subsequent cooling to M_s temperature. As it was already shown in [36], the deformation process is associated with a serious strain hardening for all alloys. Reorientation of the thermal-induced martensite (room temperature deformation) and formation of the stress-induced martensite (M_s deformation) are accompanied by plastic deformation, realized by the dislocation slip. Meng et al. [30] observed strain hardening during the stress-induced MT in Ti–Ni–Hf well over M_s, explaining it in terms of the martensitic deformation in combination with dislocation slip on the [1 0 0] (0 0 1) slip system. It was shown [24] that the critical stress for dislocation slip of parent phase is almost the same as for the stress-induced MT in Ti–Ni–Hf. Such a behaviour becomes more clear considering findings in [22], where orientation relationship in Ti–Ni–Hf was detected as [1 0 0]B2//[1 0 0]B19′ and (0 0 1)B2//(0 1 1)B19′. The (0 0 1) compound twinning was considered as the lattice invariant shear. The formation of such a (0 0 1) compound twin involves the slip of $a/2$ on (0 0 1) martensite plane, according to [37]. In our case, we deformed austenite at exactly M_s in order to achieve the best shape recovery possible. It can be seen that irreversible deformation associated with the dislocation slip was not avoided, because the preliminary deformation of $TiNi_{49.42}Hf_{14.63}$ was 8%, while the overall recovered one (ε_R) was only 3.4% (Table 1). It seems like the same is applicable to Ti–Ni–Zr alloys because of the similar MT crystallography [38]. As for Zr–Cu-based alloys, the lattice correspondence suggested in [39] was confirmed through establishing the orientation relationship for the binary Zr–Cu shown in Fig. 2. The [1 0 0]B2//[1 0 0]B19′, (0 1 0)B2//(0 1 1)B19′ orientation relationship can be clearly seen as well as (0 1 1) twinning. So, the simultaneous formation of the stress-induced B19′ martensite and dislocation slip are definitely characteristic for Zr–Cu-based alloys, analogously to Ti–Ni–Hf.

It was possible to choose the alloys with the optimal shape recovery (Fig. 3). Overall maximal shape recovery after a deformation at M_s as well as chemical composition and MT characteristics for all optimal alloys in question are shown in Table 1.

It can be seen (Table 1) that contrary to Zr–Cu [35], MT in $ZrCu_{28.2}Ni_{6.8}Co_{15.4}$ alloy (mainly B2 → B19′) shows already some signs of thermoelastic behaviour (smaller hysteresis, $A_s < M_s$; Table 1). Still, the energy dissipated during the MT cycle ($E_d = Q^{M>A} - Q^{A>M}$, according to [40], where $Q^{M>A}$ is the heat of the reverse MT, while $Q^{A>M}$ is the heat of the forward one (Table 1)) is high as well as MT temperature intervals, compared to Ti–Ni-based alloys. The energy dissipated during MT in $ZrCu_{29.9}Ni_{11}Co_{10.2}Ti_{6.6}$ alloy (mainly B2 → Cm) is even smaller than for $TiNi_{49.42}Hf_{14.63}$ alloy but MT temperature intervals are still larger (Table 1) due to the specific formation of two martensitic phases. It also should be noted that the driving force of the MT is the highest for $TiNi_{49.42}Hf_{14.63}$, while the smallest one can be noticed for $ZrCu_{29.9}Ni_{11}Co_{10.2}Ti_{6.6}$ alloy (Table 1).

The value of the maximal shape recovery (ε_R) restored after heating and cooling back to room temperature, correlates well with the dissipated energy E_d (Table 1). The largest overall shape recovery corresponds to the smallest E_d in the case of $TiNi_{48.78}Zr_{18.21}$. On the other hand, the shape recovery on heating shows more peculiar features (Fig. 4), which are discussed in detail in [36]. It can be seen that in all alloys in question the shape recovery takes place in two stages. While the low temperature stage is associated with a slightly stabilized martensite (overheating, compared to thermal-induced MT, on shape recovery is not

Table 1
Heat exchange and temperatures for thermally induced MT in Zr–Cu- and Ti–Ni-based SMAs with maximal shape recovery (ε_R)

Composition (at.%)	M_s (K)	M_f (K)	A_s (K)	A_f (K)	$Q^{A>M}$ (J/mol)	$Q^{M>A}$ (J/mol)	E_d	ε_R (%)
$ZrCu_{28.2}Ni_{6.8}Co_{15.4}$	520	400	485	600	1318	1524	206	2.5
$ZrCu_{29.9}Ni_{11}Co_{10.2}Ti_{6.6}$	450	340	410	520	1156	1230	74	3.5
$TiNi_{48.78}Zr_{18.21}$	490	410	470	550	1569	1630	61	3.7
$TiNi_{49.42}Hf_{14.63}$	460	380	435	510	1750	1837	87	3.4

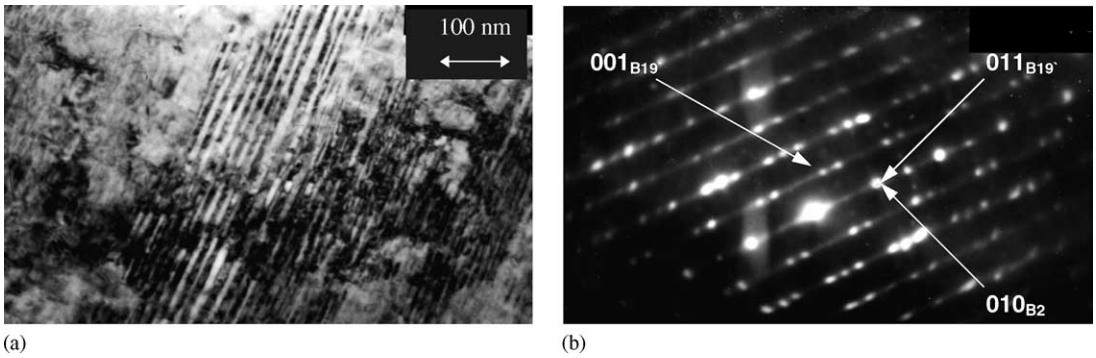

Fig. 2. Structure of the Zr–Cu compound after the 90 cycles in 77–670 K: (a) bright field from the neighboring B19′ martensite and retained B2 austenite and (b) corresponding diffraction pattern, zone axis [1 0 0].

higher than 90 K), the high-temperature stage is associated with the recrystallization process, which is triggered by the significantly deformed martensite. The similar reasoning can be found in [13], which was used to explain the influence on the reverse MT of the recrystallization in Ti–Pd–Ni alloys.

Elastic modulus of the HTSMA is also very important for shape recovery because of the necessity to accommodate the

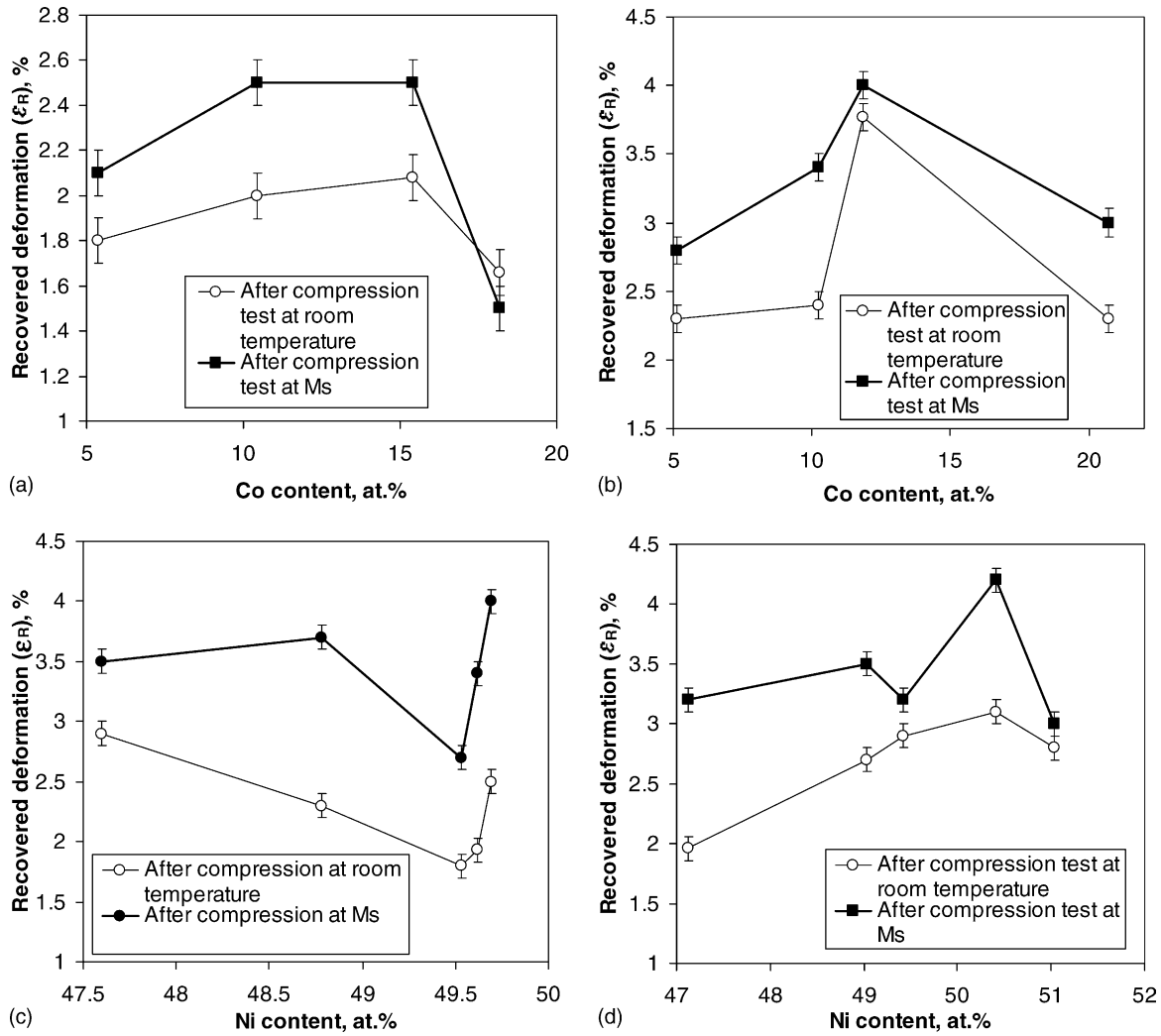

Fig. 3. Shape recovery measured by TMA vs. (a) Co content in $Zr_{50}Cu_{43-x}Ni_7Co_x$, (b) Co content in $Zr_{43}Cu_{39-x}Ni_{11}Co_xTi_7$, (c) Ni content in $Ti_{82-x}Ni_xZr_{18}$ and (d) Ni content in $Ti_{85.3-x}Ni_xHf_{14.7}$ after deformation up to 8% (after unloading).

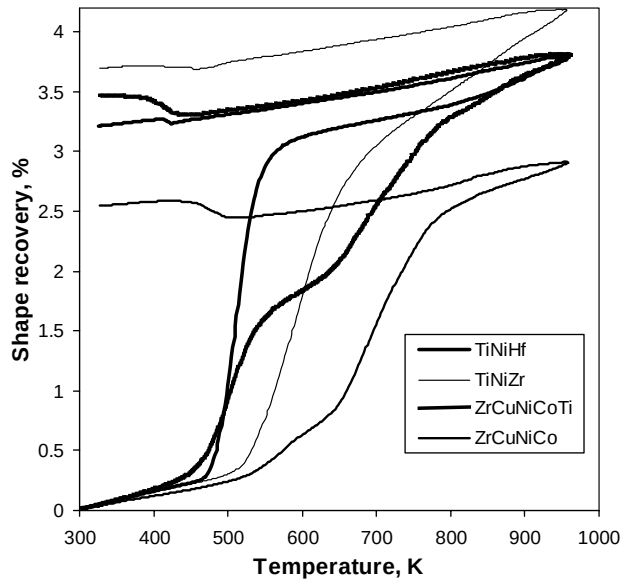

Fig. 4. Shape recovery for the optimal Zr–Cu- and Ti–Ni-based high-temperature shape memory alloys (Table 1).

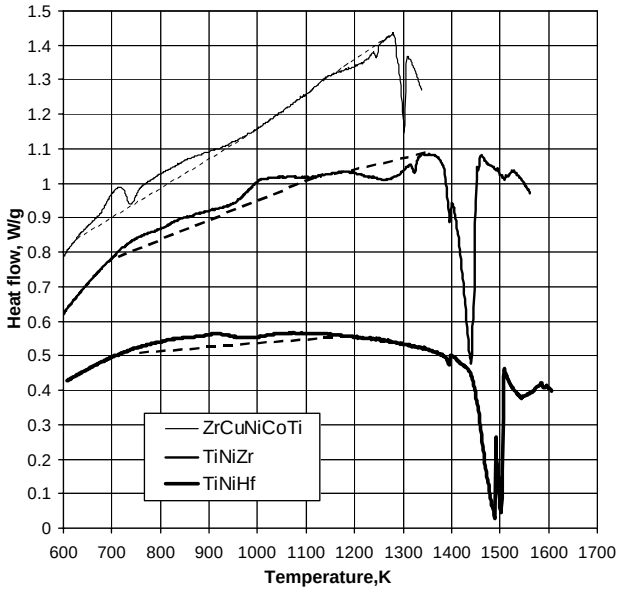

Fig. 6. Phase transformations on heating for the optimal HTSMA under study (Table 1).

MT shape change. It can be seen from Fig. 5 that the lowest elastic modulus corresponds to the best shape recovery in $TiNi_{49.42}Hf_{14.63}$ and for $ZrCu_{28.2}Ni_{6.8}Co_{15.4}$ alloy and vice versa (Figs. 4 and 5, Table 1).

The best in high-temperature shape recovery compositions (Fig. 4, Table 1) were investigated further in order to find out whether alloys in question are stable and homogeneous. The results of the high-temperature DSC are shown in Fig. 6. It is seen that all optimal HTSMA exhibited the same behavior on heating beyond 570 K. The only difference exists in the actual temperatures of the exo- and endothermic reactions.

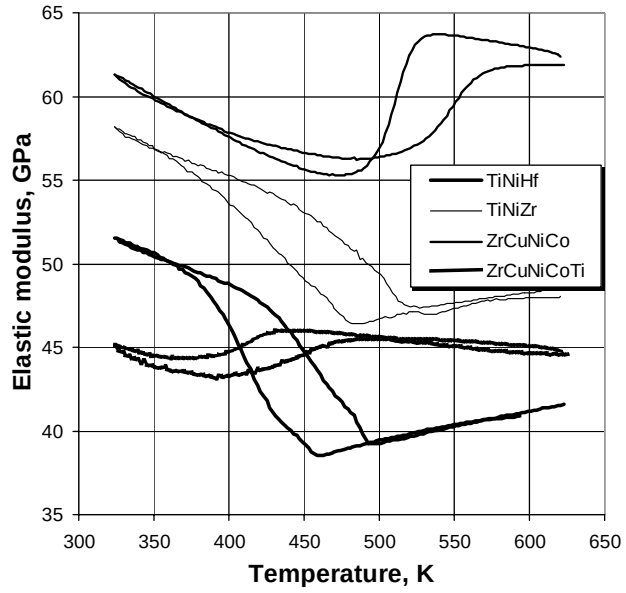

Fig. 5. Elastic modulus vs. temperature behavior of the optimal Zr–Cu- and Ti–Ni-based high-temperature shape memory alloys (Table 1).

First, a two-step exothermic transformation takes place. For the Zr–Cu-based alloy it happens in 640–970 K temperature range and for Ti–Ni–Zr and Ti–Ni–Hf alloys it takes place in 720–1120 K temperature range. The following endothermic transformation occurs in several steps with the major melting peaks at 1300 K (T_m = 1280 K) for Zr–Cu-based alloy and at 1400–1450 K (T_m = 1380 K) and 1450–1520 K (T_m = 1440 K) for Ti–Ni–Zr and Ti–Ni–Hf correspondingly. A single and sharp melting peak for Zr–Cu-based alloy testifies indirectly to a good chemical homogeneity for this material. On the contrary, in the case of Ti–Ni–Zr alloy the melting reaction has three stages at 1320, 1390 and 1440 K. Ti–Ni–Hf alloy also produces 3 stages of melting. The melting peak at 1390 K corresponds with the same one as for Ti–Ni–Zr. The following melting of Ti–Ni–Hf alloy reveals itself at 1480 and 1500 K.

High-temperature DSC studies made it possible to presume an inhomogeneity in the as-cast Ti–Ni-based alloys. Results of the SEM studies of this inhomogeneity are shown in Figs. 7 and 8.

Fig. 7 represents the results of the Ti–Ni–Zr alloy. Compositions of the phases uncovered are listed below the micrographs. According to [41–43], measured composition of the black phase corresponds to the $MgZn_2$-type ternary Laves Ψ-phase. An endothermic peak started at 1200 K on heating a Ti–Ni–Zr alloy, which must be associated with the $\Psi \Rightarrow \beta'$ solid–solid transformation, where β′ is a high-temperature cubic phase that is transforming martensitically on cooling as well as other phases mainly existing in Ti–Ni–Zr alloy. Two “grey” regions belong to one martensitic phase with a serious chemical inhomogeneity resulting in a two-step main melting peak detected by high-temperature DSC. The “white” phase along grain boundaries shown on a Fig. 7

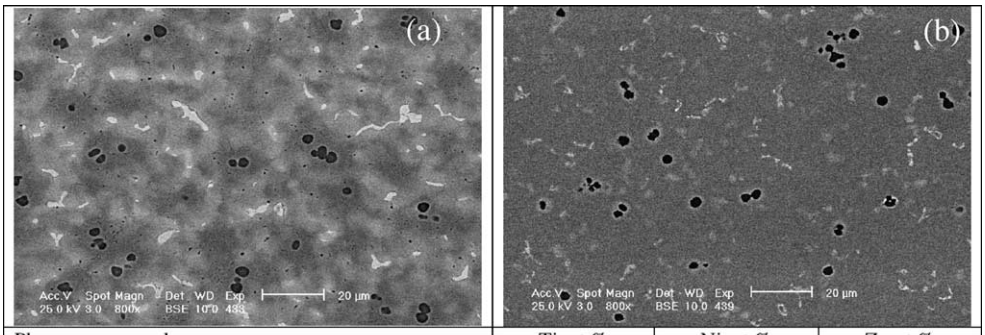

Phases uncovered	Ti, at.%	Ni, at.%	Zr, at.%
TiNiZr, as-cast, white phase	29.52	50.39	20.09
TiNiZr, as-cast, light grey region (martensite)	30.82	49.03	20.15
TiNiZr, as-cast, dark grey region (martensite)	35.01	47.19	17.8
TiNiZr, as-cast, black phase or Ψ phase	44.95	34.06	20.99

Fig. 7. SEM micrographs (back-scattered electrons) for the $TiNi_{48.78}Zr_{18.21}$ alloy taken in the as-cast (a) and annealed (b; 1270 K, 1 h) states and compositions of the phases uncovered.

melts at lower temperature and can be of a Heusler type but this suggestion needs a more detailed further investigation. The homogenization annealing at 1270 K for 1 h resulted in equalization of the chemical composition of the inhomogeneous β′-phase and in the beginning of the dissolution of the possible Heusler phase (Fig. 7b).

Microstructural state of the Ti–Ni–Hf alloy, shown in Fig. 8, looks very similar to the case of Ti–Ni–Zr. However, some important differences exist between those microstructures.

There are two phases located at the grain boundaries: Heusler phase and $NiTi_2$-type π′-phase. The main phase (β′-phase already tranformed to martensite) contains two components similar to the Ti–Ni–Zr. The homogenization annealing at 1270 K for 1 h resulted in equalization of the chemical composition of the inhomogeneous β′-phase also similar to Ti–Ni–Zr. However, 1 h of annealing was enough for the disappearance of the white Heusler phase. Unfortunately, such annealing did not affect π′-phase as can be seen in Fig. 7b. High-temperature DSC also did not show any sign of the solid–solid transformation of this phase particles to the β′-phase as it happened in the Ti–Ni–Zr case.

The formation of the Ψ- and π′-phases in Ti–Ni–Zr and Ti–Ni–Hf alloys correspondingly can cause the degradation of the mechanical characteristics, make these alloys very brittle and should therefore be avoided.

The thermal cycling influence was studied with the help of DSC measurements in the 370−670 K temperature range with a 5 K/min heating–cooling rate. The results for the optimal high-temperature shape memory alloys (HTSMA) are shown in Figs. 9–11. For the case of the thermal cycling of the Zr–Cu-based optimal alloy, it can be clearly seen that the temperatures of the reverse MT are quite stable and are not changed much during 40 thermal cycles (Fig. 9). Temperatures of the forward MT decrease about 30 K and then stabilize after 40 thermal cycles. The best Ti–Ni–Zr alloy exhibits a decrease in all MT temperatures on thermal cycling (Fig. 10). The actual amount of the decrease is 35 K

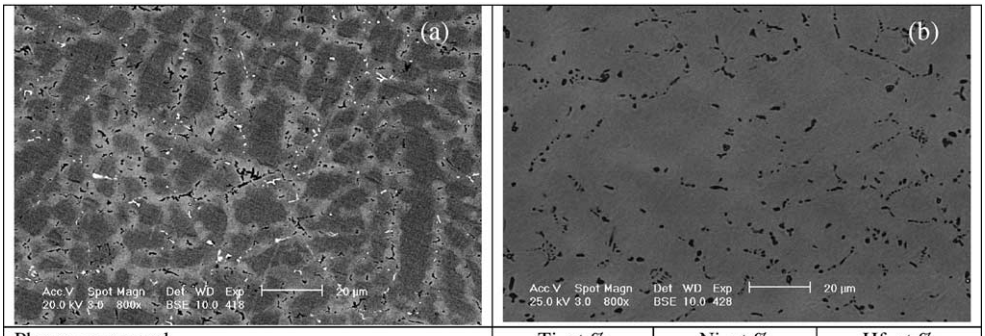

Phases uncovered	Ti, at.%	Ni, at.%	Hf, at.%
TiNiHf, as-cast, white phase	25.45	49.89	24.66
TiNiHf, as-cast, light grey region (martensite)	35.26	49.24	15.50
TiNiHf, as-cast, dark grey region (martensite)	37.06	48.85	14.09
TiNiHf, as-cast, black phase or π` phase	59.16	31.15	9.69

Fig. 8. SEM micrographs (back-scattered electrons) for the $TiNi_{49.42}Hf_{14.63}$ alloy taken in the as-cast (a) and annealed (b; 1270 K, 1 h) states and compositions of the phases uncovered.

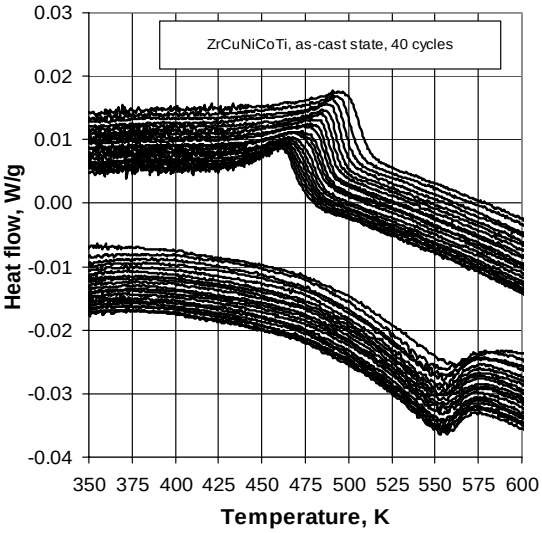

Fig. 9. MT behavior for the $ZrCu_{29.9}Ni_{11}Co_{10.2}Ti_{6.6}$ alloy detected by DSC on thermal cycling.

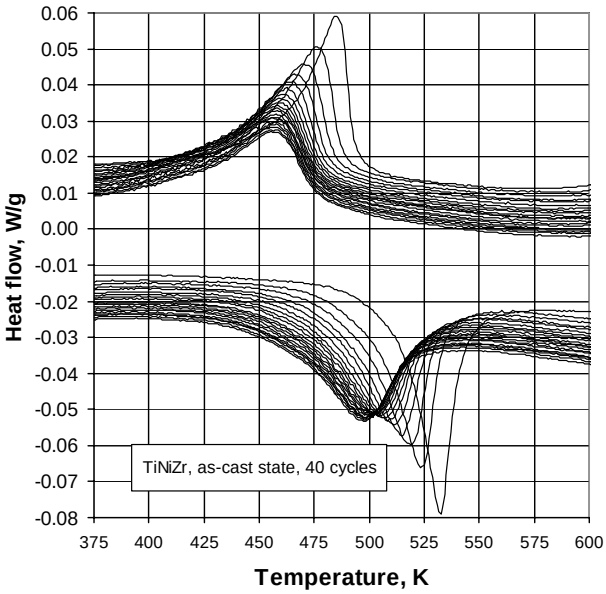

Fig. 10. MT behavior for the $TiNi_{48.78}Zr_{18.21}$ alloy detected by DSC on thermal cycling.

but 40 thermal cycles are quite enough for the stabilization of MT temperatures.

The best Ti–Ni–Hf alloy in as-cast condition undergoes multi-step MT that was attributed earlier to the chemical inhomogeneites in this material. On thermal cycling the forward MT shifts to lower temperatures by not more than 15 K keeping its multi-step behavior. The sharp peak of the reverse MT decreases by 30 K and stabilized as a multi-step extended peak after 40 thermal MT cycles (Fig. 11a).

The thermal treatment of 1270 K, 1 h was enough to equalize the composition of Ti–Ni–Hf alloy almost completely. As it can be seen form Fig. 11b, the forward MT peak has a much narrower interval as well as the peak of the reverse MT. Nevertheless, after 40 thermal cycles the forward MT in Ti–Ni–Hf alloy becomes multi-stage again.

On the contrary, the reverse MT peak remains sharp after 40 thermal cycles. Actual stabilization of MT temperatures in homogenized Ti–Ni–Hf alloy takes place after 10–15 thermal cycles.

It can be concluded that all alloys studied are relatively stable to thermal cycling in the 370–670 K temperature range. The most stable is Zr–Cu-based alloy. Its reverse MT is not affected by thermal cycling at all (Fig. 9).

The comparative oxidation resistance studies of all optimal HTSMA in question were carried out with the help of thermogravimetry. The results are shown in Fig. 12. It can be seen that comparing to binary Ti–Ni [44] or Ti–Pd–Ni [16] the most stable to oxidation is Ti–Ni–Hf alloy. It shows

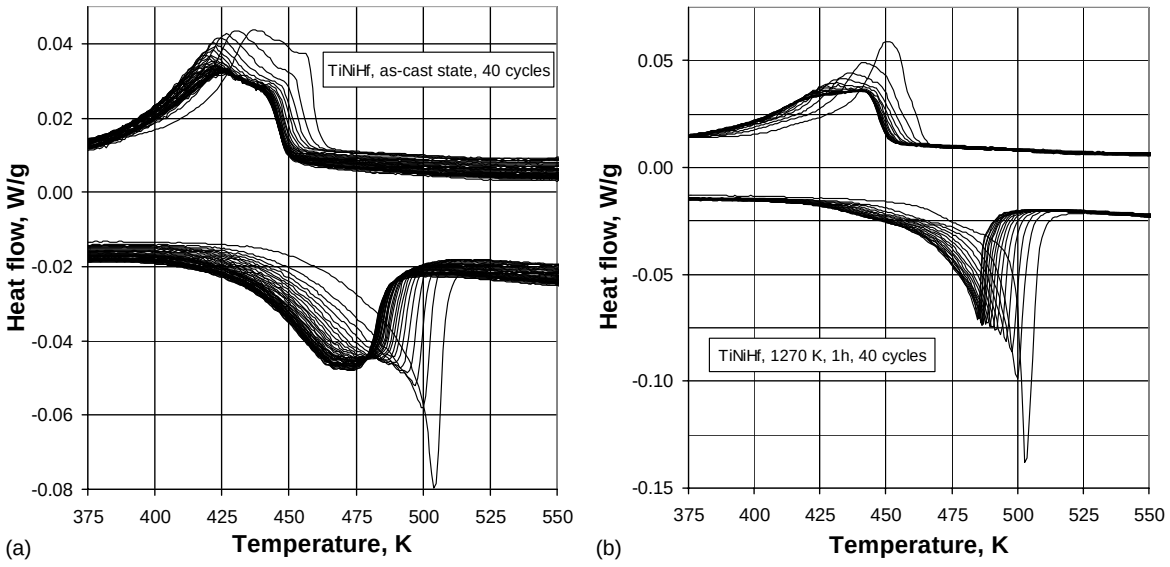

Fig. 11. MT behavior for the $TiNi_{49.42}Hf_{14.63}$ alloy detected by DSC on thermal cycling ((a) as-cast and (b) 1270 K, 1 h).

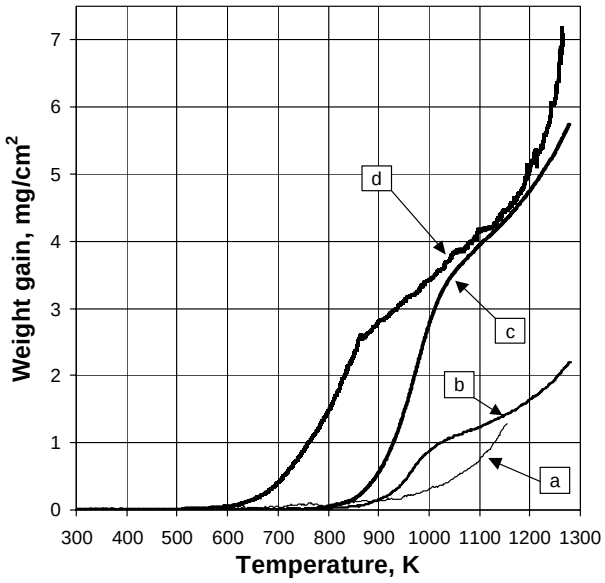

Fig. 12. Oxidation of the Ti–50 at.% Ni (a), $TiNi_{49.42}Hf_{14.63}$ (b), $TiNi_{48.78}Zr_{18.21}$ (c) and $ZrCu_{29.9}Ni_{11}Co_{10.2}Ti_{6.6}$ (d) on heating in DuPont 951 TGA with the rate 1 K/min and under 50 ml/min air flow.

more pronounced stage of the Ni segregation to the surface. Then, above 1070 K, it tends to oxidize even less than binary Ti–Ni (Fig. 12). Ti–Ni–Zr optimal HTSMA is more affected by oxidation, though the oxidation behavior is quite similar to Ti–Ni–Hf case. Zr–Cu-based optimal HTSMA starts to oxidize at lower temperatures (around 620 K) showing the same intensity and behavior of oxidation as Ti–Ni–Zr alloy.

4. Conclusion

Summarizing, Ti–Ni–Hf alloy remains at the moment the most attractive inexpensive candidate for high-temperature shape memory applications. The observed thermal cycling stabilization for it is within an acceptable range of thermal cycles and no serious degradation in transformation temperatures was observed. Moreover, it is possible to improve the thermal stability of Ti–Ni–Hf alloy by a homogenization treatment, as can be seen in Fig. 11. It should be fairly noted, that there are already some publications indicating that the long-term aging in the martensite leads to significant martensite stabilization [21,25] in Ti–Ni–Hf, for example. It means that precipitation processes should be applied to HTSMA in austenitic state in advance to prevent martensite stabilization not only in a sense of decomposition but also to prevent plastic deformation by slip during the deformation prior to shape recovery.

As for the shape recovery, it has to be noted that the most attractive material is again Ti–Ni–Hf, because its first stage shape recovery, associated with reverse MT, has the narrowest temperature interval and the larger amount of 3.1% of the shape recovery at this stage (Fig. 4). Taking into account the deformation recovered with the help of recrystallization processes, it is clear that about 0.8% of the recoverable strain can be added to the existing amount if the necessary strengthening to avoid plastic deformation by slip can be achieved. The same is true for Ti–Ni–Zr, where the maximal overall shape recovery was achieved (Table 1). Additional strengthening of some kind should narrow the temperature intervals of shape recovery and add more than 1% of the recoverable deformation to the existing one.

As for Zr–Cu-based alloys, it is clear that preferential (or only) formation of Cm martensite can improve the shape recovery of this material. Moreover, it has to be noted that, under conditions of the formation of only one Cm martensite and avoiding of the plastic deformation by slip, it could be possible to obtain the same amount of shape recovery in a narrow temperature interval of the reverse MT as in Ti–Ni–Hf alloys. On the other hand, once Ti–Ni–Zr and Ti–Ni–Hf compositions exhausted already their potential in a sense of further increase of the temperatures of shape recovery, Zr–Cu-based alloys can be adjusted easily up to 1000–1100 K by alloying [7,34]. The same is possible only with the help of a few very expensive materials [1–5,8–10]. Another important attractive feature of Zr–Cu-based alloys is the fact that they are so-called linear intermetallic compounds, just like the binary Zr–Cu [42,43] and precipitation of intermetallic phases on grain boundaries (like in Ti–Ni–Zr and Ti–Ni–Hf) is less probable if one can maintain quasibinary stoichiometry.

Finally, it has to be noted that for the most HTSMA, MT of B2 austenite results in orientation relationship between austenite and martensite, which is becoming closer to the Bain correspondence with the increase of MT temperatures. It can be seen for Ti–Ni–Hf [22], Zr–Cu (Fig. 2) and even for Ti–Ni–Pd alloy system [45], where at 25 at.% of Pd the invariant plane was found to be (0 0 1) basal one for B19 martensite. As the lattice invariant shear in this case becomes (0 0 1) compound twinning, the dislocation slip during MT is inevitable according to [37]. This is the reason why the critical stress for dislocation slip is almost the same as for the stress-induced MT in Ti–Ni–Hf [24]. That is why the strain hardening level (martensite stabilization by plastic deformation) is so high for all HTSMA in question [30,36]. Unfortunately, there are not so many possibilities to improve the situation. In fact, only precipitation hardening to prevent plastic deformation looks feasible enough. It was applied already with some success to Ti–Pd–Ni HTSMA [3]. Solution hardening is unlikely to be an option because it is always associated with bonding enhancement, which stabilizes the high-temperature B2 phase or, in other words, decreases MT temperatures [46,47]. In this regard, exploitation of the highly ordered monoclinic martensite belonging to *Cm* space group [39] in Zr–Cu-based alloys looks promising because one can expect the change in orientation relationship in this case. The plane (0 1 1) of Cm martensite cannot match the (0 1 0) plane of austenite as it is happening for B19′ martensite (Fig. 2).

References

[1] J. Beyer, J.H. Mulder, in: Proceedings of the Advanced Materials'93, vol. 18B, Transaction Material Research Society of Japan, 1994, pp. 1003–1008.
[2] J. Van Humbeeck, Transactions of ASME, J. Eng. Mater. Tech. 121 (1999) 98–101.
[3] K. Otsuka, X. Ren, Intermetallics 7 (1999) 511–528.
[4] Y.N. Koval, Mater. Sci. Forum 327328 (2000) 271–278.
[5] Y.N. Koval, G.S. Firstov, J. Van Humbeeck, L. Delaey, W.Y. Jang, J. Phys. IV C8 (5) (1995) 1103–1108.
[6] G.S. Firstov, Yu.N. Koval, J. Van Humbeeck, J. Phys. IV C5 (7) (1997) 549–554.
[7] G.S. Firstov, J. Van Humbeeck, Y.N. Koval, in: Proceedings of the SMST'99, CD "SMST-99: Shape Memory and Superelastic Technologies" by SMST Europe, 1999, pp. 446–450.
[8] R.W. Fonda, H.N. Jones, R.A. Vandermeer, Scripta Mater. 39 (8) (1998) 1031–1037.
[9] R.W. Fonda, H.N. Jones, Mater. Sci. Eng. A 273–275 (1999) 275–279.
[10] Z.R. He, J.E. Zhou, Y. Furuya, Mater. Sci. Eng. A 348 (1–2) (2003) 36–40.
[11] Y.Q. Ma, C.B. Jiang, G. Feng, H.B. Xu, Scripta Mater. 48 (2003) 365–369.
[12] D. Golberg, Y. Xu, Y. Murakami, S. Morito, K. Otsuka, T. Ueki, H. Horikawa, Intermetallics 3 (1995) 35–46.
[13] Y. Xu, K. Otsuka, T. Ueki, K. Mitose, Mater. Res. Soc. Symp. Proc. 459 (1997) 413–418.
[14] W. Cai, K. Otsuka, Scripta Mater. 41 (12) (1999) 1311–1317.
[15] T. Sawaguchi, M. Sato, A. Ishida, Mater. Sci. Eng. A 332 (2002) 47–55.
[16] Q.C. Tian, J. Chen, Y. Chen, J. Wu, Z. Metallkd. 94 (2003) 36–40.
[17] K. Mizuuchi, K. Inoue, K. Hamada, K. Yamauchi, K. Enami, M. Sugioka, M. Itami, Y. Okanda, Mater. Sci. Eng. A 329–331 (2002) 557–562.
[18] V.P. Sivokha, L.L. Meisner, Physica B 296 (2001) 329–333.
[19] G.E. Monastyrsky, V. Odnosum, J. Van Humbeeck, V.I. Kolomytsev, Yu.N. Koval, Intermetallics 10 (2002) 95–103.
[20] G.E. Monastyrsky, J. Van Humbeeck, V.I. Kolomytsev, Yu.N. Koval, Intermetallics 10 (2002) 613–624.
[21] S.F. Hsieh, S.K. Wu, Mater. Characterization 45 (2000) 143–152.
[22] X.D. Han, W.H. Zou, R. Wang, Z. Zhang, D.Z. Yang, Acta Mater. 44 (9) (1996) 3711–3721.
[23] X.D. Han, R. Wang, Z. Zhang, D.Z. Yang, Mater. Lett. 30 (1997) 23–28.
[24] Y.Q. Wang, Y.F. Zheng, W. Cai, L.C. Zhao, Scripta Mater. 40 (12) (1999) 1327–1331.
[25] R. Santamarta, C. Seguí, J. Pons, E. Cesari, Scripta Mater. 41 (8) (1999) 867–872.
[26] P. Shloßmacher, H. Rösner, A.V. Shelyakov, in: Proceedings of the SMST'99, CD "SMST-99: Shape Memory and Superelastic Technologies" by SMST Europe, 1999, pp. 428–432.
[27] C. Zhang, P.E. Thoma, R. Zee, Mater. Res. Soc. Symp. Proc. 604 (2000) 129–134.
[28] X.L. Meng, Y.F. Zheng, Z. Wang, L.C. Zhao, Scripta Mater. 42 (2000) 341–348.
[29] X.L. Meng, W. Cai, L.M. Wang, Y.F. Zheng, L.C. Zhao, L.M. Zhou, Scripta Mater. 45 (2001) 1177–1182.
[30] X.L. Meng, W. Cai, Y.F. Zheng, Y.X. Tong, L.C. Zhao, L.M. Zhou, Mater. Lett. 55 (2002) 111–115.
[31] J. Font, E. Cesari, J. Muntasell, J. Pons, Mater. Sci. Eng. A 354 (2003) 201–211.
[32] G. Roebben, B. Bollen, A. Brebels, J. Van Humbeeck, O. Van der Biest, Rev. Sci. Instrum. 68 (1997) 4511–4515.
[33] A.S. Nowick, B.S. Berry, Anelastic Relaxation in Crystalline Solids, Academic Press, New York, 1972.
[34] Yu.N. Koval, G.S. Firstov, L. Delaey, J. Van Humbeeck, Scripta Met. Mater. 31 (7) (1994) 799–802.
[35] G.S. Firstov, J. Van Humbeeck, Yu.N. Koval, J. Phys. IV, Part 8 11 (2001) 481–486.
[36] G.S. Firstov, J. Van Humbeeck, Yu.N. Koval, Scripta Mater. 50 (2004) 243–248.
[37] Y. Kudoh, M. Tokonami, S. Miyazaki, K. Otsuka, Acta Metall. 33 (1985) 2049–2056.
[38] J.H. Mulder, Investigation of High Temperature Shape Memory Alloys from the Ni–Ti–Zr and Ni–Ti–Hf Systems, Ph.D. Thesis, University of Twente, 1995, p. 142.
[39] D. Schryvers, G.S. Firstov, J.W. Seo, J. Van Humbeeck, Yu.N. Koval, Scripta Mater. 36 (10) (1997) 1119–1125.
[40] J. Ortin, A. Planes, Acta Metall. 36 (8) (1988) 1873–1889.
[41] K.P. Gupta, J. Phase Equilib. 20 (4) (1999) 441–448.
[42] D. Arias, J.P. Abriata, Bull. Alloy Phase Diagrams 11 (5) (1990) 452–459.
[43] K.-J. Zeng, M. Hämäläinen, H.L. Lukas, J. Phase Equilib. 15 (6) (1999) 577–586.
[44] G.S. Firstov, R.G. Vitchev, H. Kumar, B. Blanpain, J. Van Humbeeck, Biomaterials 23 (2002) 4863–4871.
[45] V.N. Khachin, Rev. Phys. Appl. 24 (1989) 733–739.
[46] G.S. Firstov, J. Van Humbeeck, Yu.N. Koval, R.G. Vitchev, J. Phys. IV 112 (2003) 1075–1078.
[47] S.A. Shabalovskaya, in: C.M. Wayman, J. Perkins (Eds.), Proceedings of the ICOMAT-92, Monterey, USA, 20–24 July 1992, Monterey Institute for Advanced Studies, 1993, pp. 123–128.